Excitation polarization-independent photo-induced restoration of inversion symmetry in Td-WTe

Aoki, Ryota; Uchida, Kento; Tanaka, Koichiro

AIP Advances

Excitation polarization-independent photo-induced restoration of inversion symmetry in Td-WTe_2

Cite as: AIP Advances **12**, 045309 (2022); https://doi.org/10.1063/5.0086398
Submitted: 26 January 2022 • Accepted: 07 March 2022 • Published Online: 07 April 2022

Ryota Aoki, Kento Uchida and Koichiro Tanaka

AIP Advances ARTICLE scitation.org/journal/adv

Excitation polarization-independent photo-induced restoration of inversion symmetry in Td-WTe_2

Cite as: AIP Advances 12, 045309 (2022); doi: 10.1063/5.0086398
Submitted: 26 January 2022 • Accepted: 7 March 2022 •
Published Online: 7 April 2022

Ryota Aoki,[1] Kento Uchida,[1,a)] and Koichiro Tanaka[1,2,a)]

AFFILIATIONS

[1] Department of Physics, Graduate School of Science, Kyoto University, Kyoto 606-8502, Japan
[2] Institute for Integrated Cell-Material Sciences (WPI-iCeMS), Kyoto University, Kyoto 606-8501, Japan

[a)] **Authors to whom correspondence should be addressed:** uchida.kento.4z@kyoto-u.ac.jp and kochan@scphys.kyoto-u.ac.jp

ABSTRACT

Td-WTe_2 is a topologically nontrivial material and exhibits a variety of physical properties, such as giant unsaturated magnetoresistance and the unconventional thermoelectric effect, due to its topological nature. It is also known to exhibit ultrafast topological phase transitions that restore its inversion symmetry by intense terahertz and mid-infrared pulses, and these properties demonstrate the possibility of ultrafast control of devices based on topological properties. Recently, a novel photo-induced topological phase transition by using polarization-controlled infrared excitation has been proposed, which is expected to control the material topology by rearranging the atomic orbitals near the Weyl point. To examine this topological phase transition, we experimentally studied the excitation-polarization dependence of the infrared-induced phase dynamics in a thin-layer of Td-WTe_2. Time-resolved second harmonic generation (SHG) measurements showed that SHG intensity decreases after the infrared pump regardless of the polarization. Polarization-resolved infrared pump–probe measurements indicated that the polarization-selected excited state relaxes quite rapidly (i.e., within 10–40 fs). Considering these experimental results, we conclude that it is difficult to control the photo-induced phase transition through orbital-selective excitation owing to the rapid loss of carrier distribution created by polarization-selective excitation in thin-layer Td-WTe_2 under our experimental condition. These results indicate that the suppression of the electron scattering process is crucial for experimentally realizing the photo-induced phase transition based on the polarization selection rule of the materials.

Crystalline solids having a band structure with nontrivial geometry are called topological materials, and they can be classified by their topological invariants, which differ from that of ordinary metals and insulators.[1–4] Topological materials exhibit an edge or surface state that is topologically protected against disorder, and they show unique physical properties determined by the topological invariant. Controlling those topological properties is a crucial problem for producing the next-generation of electronic devices. One method for controlling such topological properties is optical-pulse excitation.[5–12] For example, several photo-induced methods for controlling topological properties have been reported, such as controlling the gap in the Dirac node[7] in a Dirac semimetal and controlling the photo-induced Hall effect in graphene.[8,9] However, the number of experimental examples is limited.[7,8,11,12] Comprehending the details of topological phase transitions in individual materials experimentally is, therefore, of paramount importance for the adaptation of controlling topological properties to a wide range of systems.

Td-WTe_2 is a layered van der Waals material with stacking along the *c* axis, and it has in-plane *a* and *b* axes orthogonal to each other as shown in Fig. 1(a).[11,13] The Td phase of WTe_2 is a type of topological material called "non-centrosymmetric type-II Weyl semimetal,"[14–17] which is characterized by the presence of pairs of Weyl points with opposite chirality and linear band dispersion around them.[3] Due to the existence of Weyl points, WTe_2 exhibits properties such as giant unsaturated magnetoresistance,[18] an unconventional Nernst effect,[19] and an anomalous Hall effect.[20,21]

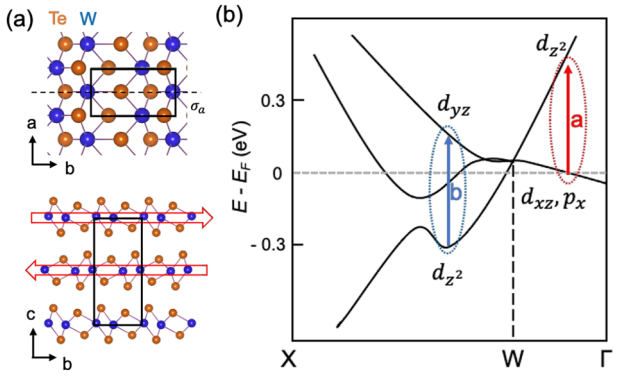

FIG. 1. (a) Crystal structure of Td-WTe_2. The unit cell is indicated by solid rectangles. The direction in which inversion symmetry is restored is shown by the red arrows. These images were generated by using VESTA.[13] (b) Schematic of orbital-selective excitation.[27] The main atomic orbitals involved in excitation with photon energy of 0.5–0.8 eV are labeled. The right-side and left-side arrows in the diagram represent the transitions with linearly polarized light along the *a* and *b* axes, respectively. This diagram is adapted from Guan *et al.*, Nat. Commun. **12**, 1885 (2021). Copyright 2021 Author(s).

On the contrary, the metastable 1T′ phase in WTe_2 has inversion symmetry and is a topologically trivial metal with no Weyl point.[22] Although it is difficult to realize the topological phase transition from Td to 1T′ phase by changing static parameters, such as pressure[23] and temperature,[24] it can be relatively easily induced through optical-pulse excitation.[11,25] This phase transition was first observed in an experiment using THz pulses by Sie *et al.*[11] They suggested that inducing a shear displacement in the direction of the arrows, as shown in Fig. 1(a), which corresponds to the normal coordinate of the shear mode at 0.23 THz, is the dominant factor in this phase transition. The same transitions were also reported to occur with mid-infrared[11] and visible[25] photoexcitation. A similar material, namely, $MoTe_2$, shows a bidirectional Td-1T′ phase transition;[26] however, WTe_2 only shows a Td-to-1T′ phase transition. Recently, it is predicted that a novel transition to a topologically distinct phase with enhanced non-centrosymmetric order may occur under different excitation conditions by Guan *et al.*[27]

The way to achieve a novel phase transition is directly linked to so-called "orbital-selective excitation,"[27] which can be understood as a kind of pleochroism.[28] For example, in a crystal with transition metal ions, the degenerated d-orbitals are split by the crystal field. The selection rule for the transition between the split orbitals (d–d transition) is determined by the symmetry of the orbitals and the direction of linear polarization. These transitions result in the changes in material color when observed at different angles because the photon energy absorbed differs according to the polarization,[29] and it has been confirmed to occur in many solid crystals.[28] Orbital-selective excitation[27] also reflects the symmetry of the orbitals before and after the transition; however, it differs in that it utilizes the topological property of band inversion near the Weyl points. This property allows polarization-selective exclusive excitation at different regions in the k-space for the same photon energy in the infrared region (0.5–0.8 eV). A schematic band structure near the Weyl point[27] is shown in Fig. 1(b).The arrows indicate the allowed transitions at a photon energy of 0.5–0.8 eV for Fermi energy level E_F. For transitions along W-Γ, according to their theoretical calculation,[27] the valence band is mainly composed of d_{xz} and p_x, and the conduction band is mainly composed of d_{z^2}. The transition-matrix elements are, therefore, finite for linear polarization along the *a* axis, while the transition is forbidden for that along the *b* axis. In contrast, along X–W, excitation with linear polarization along the $a(b)$ axis is forbidden (allowed). Such orbital-selective excitation should realize a different carrier distribution that may promote a differently directed shear displacement.[27] As a result, the excitation polarization along the *a* axis is expected to restore the inversion symmetry, which is a conventional transition, while that along the *b* axis may cause a phase transition that enhances the intrinsic non-inversion symmetric order. This newly proposed phase is topologically different from Td and 1T′ phases because the annihilation of the Weyl points occurs in a different way than restoring the inversion symmetry. The previous study has reported the restoration of the inversion symmetry isotropic to the excitation polarization in terahertz or far-infrared region, where the orbital-selective excitation is not effective.[11] However, neither the excitation-polarization dependence in the infrared region, where the orbital-selective rule is valid, nor the phase transition caused by orbital-selective excitation has been reported. In addition, it is non-obvious how the scattering mechanism works for the orbital selectively excited carrier distribution.

In this study, to verify photo-induced phase-transition dynamics reflecting the orbital-selective excitation, we conducted time-resolved second-harmonic generation (TR-SHG) measurements[30] with polarization-controlled infrared excitation. The excitation photon energy was taken near the Weyl point between 0.5 and 0.8 eV in order to satisfy the orbital selection rule. We found that only the transition that restores the inversion symmetry occurs regardless of the excitation polarization under certain experimental conditions. To investigate the origin of the excitation polarization-independent transition, we first used infrared pump–probe measurement to determine the timescale over which an anisotropic carrier distribution depending on the excitation polarization is maintained. Then, we estimated the relaxation time by the discrete four-level model to be about 10–40 fs. Based on these two experimental results, we concluded that the orbital-selective phase transition cannot be realized due to rapid inter-orbital relaxation.

We prepared a thin-layer Td-WTe_2 sample by mechanical exfoliation technique from the bulk crystal purchased from 2D Semiconductors and transferred it onto a synthetic quartz substrate. We used the sample whose thickness is thinner than the penetration depth ($\delta \sim 100$ nm) of infrared light[31–34] so that it was possible to excite the sample uniformly. To prevent sample degradation,[35,36] we used a home-built vacuum chamber to keep the sample under vacuum during experiments. The point group of the thin-layer Td-WTe_2 is C_s because the symmetry operation with translation (: C_2, σ_b) is broken at the surface.[37,38] Therefore, we determined the in-plane crystal orientation by using symmetry analysis of SHG polarization[39] for normal incidence[20,40] (see the supplementary material, Fig. S3). On the other hand, the point group of the thin-layer 1T′-WTe_2 is C_{2h}, which is considered to be the metaphase when the inversion symmetry is restored by the photoexcitation. Since the C_{2h} has an inversion center, SHG is prohibited for any in-plane polarization direction for normal incidence.

To clarify whether an orbital-selective photo-induced phase occurs, first, we measured the changes in SHG intensity after infrared excitation. Since the SHG is sensitive to the presence or absence of the inversion symmetry of the crystal, TR-SHG measurement is an effective tool for probing changes in non-centrosymmetric order during the phase transition.[11] A schematic diagram of the experimental setup for TR-SHG measurement is shown in Fig. 2(a). The laser source is a Ti:sapphire regenerative amplifier (pulse width: 35 fs; center wavelength: 800 nm; and repetition rate: 1 kHz). Pulses with photon energies of 0.57 eV ("idler") and 0.99 eV ("signal") were simultaneously generated by using an optical parametric amplifier (OPA) (Light Conversion TOPAS-C). The photon energy of the idler was set in the region where the orbital-selective excitation is expected. The idler was used as an excitation pulse to induce the phase transition, and the signal was used as a probe pulse for SHG. The time resolution of the measurement setup was estimated to be ~220 fs (full width at half maximum, FWHM) from the cross correlation measurements between the pump pulse and the probe pulse in a thin GaSe crystal. To generate the expected orbital-selective excitation, the polarization of the idler was controlled to be parallel to the *a* or *b* axis. The polarization of the probe pulse was set parallel to the *b* axis, and only the SHG of the probe pulse was detected by a Si-CCD camera (DU920P-OE, Newton) equipped with a spectrometer (Kymera 193i, Andor). In Td-WTe_2, Fermi energy shifts by ~50 meV from room temperature to a temperature below 170 K.[41] To perform the experiment under the condition assumed by the theory,[27] the sample temperature was set to be 11 K.

Time-delay dependences of change in the SHG intensity for the two (*a* and *b* axes-parallel) excitation polarizations at photon energy of 0.57 eV are shown in Fig. 2(b). According to the figure, the SHG intensity decreases by about 50%–60% for both (*a* and *b* axes-parallel) excitation polarizations. This result agrees with that in the case of excitation with photon energy of 1.55 eV (see the supplementary material, Fig. S4), at which the orbital-selective excitation is not expected to occur.[27] We also observed oscillation of the signals, which is attributed to coherent phonon generation. When a certain phonon displacement Q is induced by the infrared pump, the SHG intensity polarized along the i axis $I_i(2\omega)$ is given as follows:[30]

$$I_i(2\omega) \propto \left|\chi^{(2)}_{ijk}(2\omega)\right|^2 + \mathrm{Re}\left[\chi^{(2)}_{ijk}(2\omega)^*\left(\frac{\partial\chi^{(2)}_{ijk}(2\omega)}{\partial Q}\right)\right]Q(t), \quad (1)$$

where $\chi^{(2)}$ is the second-order nonlinear susceptibility, and $\left(\frac{\partial\chi^{(2)}}{\partial Q}\right)$ is proportional to the hyper-Raman tensor. Since the oscillation component of the second term in Eq. (1) is sufficiently small (ΔSHG_{osc}/SHG ~ 0.05), the higher-order contributions of Q in the SHG signal are negligible, i.e., oscillation of the SHG signal directly reflects the coherent phonon motion. The observed oscillation frequency (~0.2 THz) in Fig. 2(c) is attributed to the 0.23 THz shear mode.[11,42] When this shear mode is displaced in the direction that enhances non-centrosymmetric order, the phase of oscillation is shifted by π compared to that when the inversion symmetry is restored; that is, the adjacent layers start to move in the directions opposite to the arrows, as shown in Fig. 1(a). Nevertheless, as shown in Fig. 2(c), the observed relative phases are in agreement regardless of excitation polarization. According to these results, we conclude that the polarization of the infrared pump cannot be easily used for controlling the photo-induced phase transition under the above-described experimental condition. Only the transition to the phase that restores the inversion symmetry[11,25] occurs regardless of polarization. We also carried out the above-described experiment at room temperature (see the supplementary material, Fig. S5), and the results of the experiment were similar to those obtained at 11 K. Therefore, we conclude that the influence of the slight Fermi-energy shift (~50 meV) on the photo-induced phase transition is negligible. In addition, we investigated the pump fluence dependence of the SHG intensity (see the supplementary material, Fig. S6). The amount of decrease in the SHG intensity tends to be proportional to the pump fluence regardless of the excitation polarization, and there is no significant change in the dynamics. Such a pump fluence dependence of the SHG intensity can be interpreted as a continuous transition from the Td to the 1T′ phase due to the displacement of the equilibrium point on the energy potential related to the 0.23 THz shear mode, which is usually considered in DECP[43] or impulsive stimulated Raman scattering (ISRS)[44] model. These results suggest that no sign of a selective phase transition appears in the pump fluence range in our experiments.

Next, we performed infrared pump–probe measurement to verify the timescale over which polarization-dependent carrier distribution is maintained. The experimental setup for degenerate infrared pump–probe measurement in transmission geometry is schematically shown in Fig. 3(a). The pump and probe pulses with photon energy of 0.78 eV were generated by the OPA system, and the time resolution of the system was estimated to be

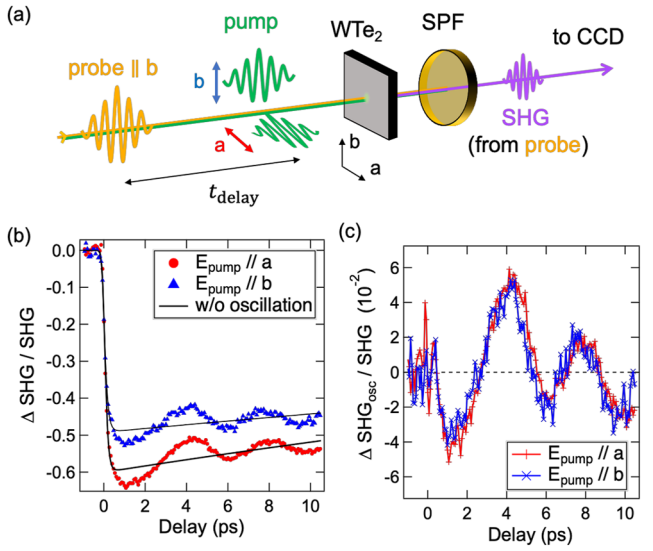

FIG. 2. (a) Schematics of TR-SHG measurement (SPF: short pass filter; CCD: charge-coupled-device camera). (b) TR-SHG measurements for different excitation polarizations with photon energy of 0.57 eV at 11 K. The probe pulse is linearly polarized along the *b* axis, and the pump fluence is 2.8 mJ/cm^2. To separate the oscillation components, a fitting function that has finite rise time decays exponentially was used (solid lines in the figure). (c) Oscillation components in transient SHG intensity.

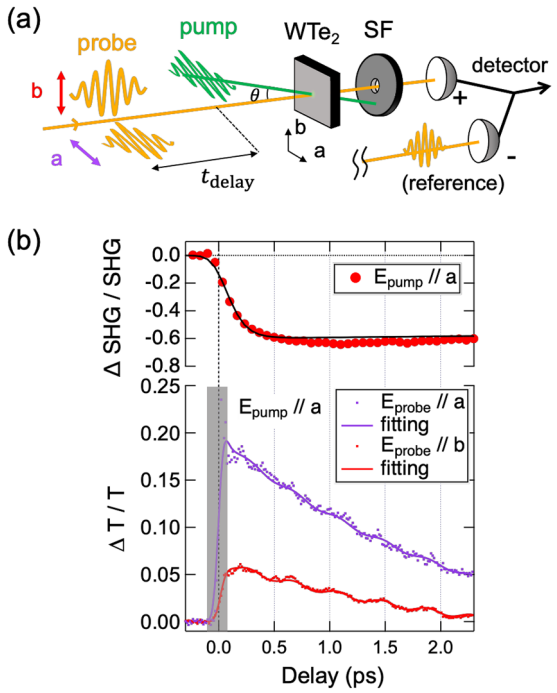

FIG. 3. (a) Schematics of the infrared pump–probe measurement in the transmission geometry (SF: spatial filter). (b) Infrared pump–probe measurements performed at room temperature. The excitation intensity is 3.2 mJ/cm^2. The fitting curve is shown by a solid line. This fitting was performed by corresponding Eqs. (3) and (4) to the results for each probe polarization, with τ_p and τ_b as common parameters. Each fitting parameter is listed in the supplementary material, Table S1. The top of the graph shows the change in the SHG intensity [as in Fig. 2(b)].

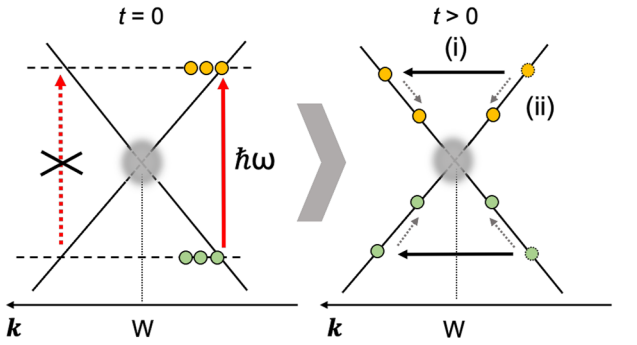

FIG. 4. Simplified view of the expected carrier dynamics in the presence of orbital-selective excitation (W: Weyl point; yellow circle: electron; green circle: hole). The figure shows the case that only the right side of the Weyl point is selectively excited for excitation polarization at $t = 0$. (i) Inter-orbital relaxation due to carrier–carrier scattering. (ii) Intra-band relaxation due to carrier–phonon scattering.

~90 fs (FWHM). An InGaAs balanced detector (1817-FS, Newport) was used to improve the signal-to-noise ratio by suppressing the common-mode noise due to laser intensity fluctuations. Since we observed no clear temperature dependence of Fermi energy in the above-described TR-SHG experiment, we performed infrared pump–probe measurements at room temperature. The time-delay dependence of transmission change $\Delta T/T$ for two probe polarizations, where the excitation pulse is linearly polarized along the a axis, is shown in Fig. 3(b). Both transmission changes tend to rise for a few tens of femtoseconds and then decay in a few picoseconds. The oscillating component should be originated from the in-plane phonon at 2.4 THz.[45] The spikes in the case of the parallel configuration contain coherent artifacts, which are discussed henceforth.

To extract the relaxation time of orbital selectively excited carriers, we consider the simplified model depicted in Fig. 4. As for this model, we assume that orbital-selective excitations can be made in Td-WTe_2. Therefore, we consider carriers are excited only in a specific band near the Weyl point (left side of the figure) initially, which depends on the excitation polarization. After that, carriers (i) spread over bands including those forbidden by orbital-selective excitation due to inter-orbital relaxation, such as carrier–carrier scattering, and (ii) relax to the metastable state by intra-band scattering via phonons. When the polarization of the probe pulse is parallel to that of the pump pulse, the peak of the transmission change due to absorption saturation may appear immediately after excitation, as also shown by conventional pump–probe measurement. In contrast to the parallel case, when the polarization of the probe pulse is perpendicular to that of the pump pulse, the absorption saturation may be delayed by the timescale of the inter-orbital scattering (right side of the figure).

To estimate the timescale over which orbital-selective excitation is maintained, we used the following fitting functions:

$$\left(\frac{\Delta T(t)}{T}\right)_a = f_a(t) * g(t) (a = \perp, \parallel), \tag{2}$$

$$f(t)_\perp = \left(1 - e^{-\frac{t}{\tau_p}}\right)\left(A_\perp e^{-\frac{t}{\tau_b}} + B_\perp + X_1(t)\right), \tag{3}$$

$$f(t)_\parallel = \left(1 + e^{-\frac{t}{\tau_p}}\right)\left(A_\parallel e^{-\frac{t}{\tau_b}} + B_\parallel + X_2(t)\right), \tag{4}$$

$$X_i(t) \propto \cos(\omega t - \phi_i) e^{-\frac{t}{\tau_{ph}}} (i = 1, 2), \tag{5}$$

where $f_a(t)$ is the response function of pump-induced change and $X_i(t)$ is the function describing coherent phonon oscillation ($\omega \simeq 2.4$ THz). To incorporate the effect of finite pulse width, the response function $f_a(t)$ was convolved with cross correlation function $g(t)$ between the pump pulse and the probe pulse. τ_p, τ_b, and τ_{ph} represent inter-orbital (momentum) relaxation time, intra-band relaxation time, and coherent phonon relaxation time, respectively. The term corresponding to B_a is introduced to describe the contribution of the metastable phase, and it is treated as an offset component since the relaxation time is very long (typically >100 ps[11]) compared to the typical timescale discussed in this paper. τ_{ph} is also fixed as 15 ps for the same reason, and this value is roughly equivalent to previous studies.[45] These formulas were obtained by solving the rate equations of a four-level model with scattering, as described in detail in the supplementary material, Sec. 4. As a result of the fitting of experimental data in Fig. 3(b), a short inter-orbital relaxation

time of $\tau_p \sim 20 \pm 6$ fs, which was less than the time resolution of the experimental setup, was obtained. On the contrary, the intra-band relaxation time is $\tau_b \sim 3.3$ ps, which is the same order of magnitude as found in previous studies.[40,46] Note that it is necessary to treat the observed peak near the time origin in Fig. 3(b) carefully in the case of the parallel polarization configuration. This is because the observed peak contains a coherent artifact due to the $\chi^{(3)}$ process between the ultrashort pulses.[47] It is difficult to extract only the carrier dynamics from the experimental data including the coherent artifact, so the area excluding that near the time origin [shaded area in Fig. 3(b)] was fitted. Therefore, the inter-orbital relaxation time is mainly determined by the fitting results in the case of the perpendicular polarization configuration, and this result does not contradict the experimental results in the case of the parallel polarization configuration. We also measured the inter-orbital relaxation time in the case of excitation polarization parallel to the *b* axis and found that $\tau_p \sim 32 \pm 9$ fs (see the supplementary material, Fig. S8), which is almost the same timescale as that in the case of *a* axis-polarized excitation. These results indicate that the dependence of anisotropic carrier distribution on excitation polarization relaxes rapidly (at least within the time resolution of the measurement setup). Since the relaxation due to carrier–carrier scattering is strongly suppressed in an ideal Weyl semimetal,[48] the observed rapid inter-orbital relaxation suggests the existence of higher-order many-body effects, scattering through impurity,[49] and multiband-induced relaxation paths in the vicinity of Fermi energy.

Henceforth, we consider the characteristic timescale of the reduction of SHG intensity. In the top of Fig. 3(b), the delay dependence of the SHG intensity is plotted on the same timescale as the pump–probe measurement. Notably, the timescale for the SHG intensity to decrease (about 300 fs) is different from the timescales of both inter-orbital relaxation and intra-band relaxation. It is also inconsistent with the quarter period of the shear mode (1.1 ps), which couples with the phase transition. This timescale suggests that the observed reduction of the SHG intensity is not just probing the displacement driven by the 0.23 THz shear mode.[43,44] Moreover, Ji *et al.*[25] also noted a rapid decrease in the transient intensity of SHG. A possible candidate for the cause of the rapid decrease in the SHG intensity is thought to be the displacement of the in-plane lattice associated with the 2–6 THz phonons.[46,50] Qi *et al.*[50] pointed out the relaxation of the in-plane Peierls distortion by pulse irradiation, and Hein *et al.*[46] mentioned the influence of high-frequency phonons on the modification of electronic structure in the early stage of phase transition. The mechanisms related to the development of the phase transition are still under debate and need to be studied in detail in future work.

In conclusion, we experimentally demonstrated that a novel phase transition due to orbital-selective excitation does not occur in Td-WTe_2 under certain experimental conditions. The time-resolved measurements of SHG show that, in contrast to the theoretical prediction, only the transition that restores the inversion symmetry occurs independently of the excitation polarization. According to the analysis of infrared pump–probe measurement, this phenomenon may be because the inter-orbital relaxation is extraordinarily fast compared to the phonon timescale involved in the phase transition. Although no polarization-dependent phase transition was observed in the present experiment, the possibility of orbital-selective excitation cannot be rejected. If the dissipation of the anisotropic electronic distribution can be suppressed with the external control,[51] it may be possible to induce the switching phenomenon utilizing inhomogeneous carrier distribution.

See the supplementary material for the details of the four-level model and additional experimental results.

This work was supported by the JSPS Grants-in-Aid for Scientific Research (Grant Nos. 17H06124, 21H05017, and 19K14632).

AUTHOR DECLARATIONS

Conflict of Interest

The authors have no conflicts to disclose.

DATA AVAILABILITY

The data that support the findings of this study are available from the corresponding authors upon reasonable request.

REFERENCES

[1] D. J. Thouless, M. Kohmoto, M. P. Nightingale, and M. den Nijs, Phys. Rev. Lett. **49**, 405 (1982).
[2] B. Q. Lv, T. Qian, and H. Ding, Rev. Mod. Phys. **93**, 025002 (2021).
[3] N. P. Armitage, E. J. Mele, and A. Vishwanath, Rev. Mod. Phys. **90**, 015001 (2018).
[4] X. Wan, A. M. Turner, A. Vishwanath, and S. Y. Savrasov, Phys. Rev. B **83**, 205101 (2011).
[5] C. P. Weber, J. Appl. Phys. **129**, 070901 (2021).
[6] T. Oka and S. Kitamura, Annu. Rev. Condens. Matter Phys. **10**, 387 (2019).
[7] C. P. Weber, M. G. Masten, T. C. Ogloza, B. S. Berggren, M. K. L. Man, K. M. Dani, J. Liu, Z. Mao, D. D. Klug, A. A. Adeleke, and Y. Yao, Phys. Rev. B **98**, 155115 (2018).
[8] J. W. McIver, B. Schulte, F.-U. Stein, T. Matsuyama, G. Jotzu, G. Meier, and A. Cavalleri, Nat. Phys. **16**, 38 (2020).
[9] T. Oka and H. Aoki, Phys. Rev. B **79**, 081406 (2009).
[10] N. Aryal, X. Jin, Q. Li, A. M. Tsvelik, and W. Yin, Phys. Rev. Lett. **126**, 016401 (2021).
[11] E. J. Sie, C. M. Nyby, C. D. Pemmaraju, S. J. Park, X. Shen, J. Yang, M. C. Hoffmann, B. K. Ofori-Okai, R. Li, A. H. Reid, S. Weathersby, E. Mannebach, N. Finney, D. Rhodes, D. Chenet, A. Antony, L. Balicas, J. Hone, T. P. Devereaux, T. F. Heinz, X. Wang, and A. M. Lindenberg, Nature **565**, 61 (2019).
[12] M. Y. Zhang, Z. X. Wang, Y. N. Li, L. Y. Shi, D. Wu, T. Lin, S. J. Zhang, Y. Q. Liu, Q. M. Liu, J. Wang, T. Dong, and N. L. Wang, Phys. Rev. X **9**, 021036 (2019).
[13] K. Momma and F. Izumi, J. Appl. Crystallogr. **44**, 1272 (2011).
[14] A. A. Soluyanov, D. Gresch, Z. Wang, Q. Wu, M. Troyer, X. Dai, and B. A. Bernevig, Nature **527**, 495 (2015).
[15] C. Wang, Y. Zhang, J. Huang, S. Nie, G. Liu, A. Liang, Y. Zhang, B. Shen, J. Liu, C. Hu, Y. Ding, D. Liu, Y. Hu, S. He, L. Zhao, L. Yu, J. Hu, J. Wei, Z. Mao, Y. Shi, X. Jia, F. Zhang, S. Zhang, F. Yang, Z. Wang, Q. Peng, H. Weng, X. Dai, Z. Fang, Z. Xu, C. Chen, and X. J. Zhou, Phys. Rev. B **94**, 241119 (2016).
[16] B. Feng, Y.-H. Chan, Y. Feng, R.-Y. Liu, M.-Y. Chou, K. Kuroda, K. Yaji, A. Harasawa, P. Moras, A. Barinov, W. Malaeb, C. Bareille, T. Kondo, S. Shin, F. Komori, T.-C. Chiang, Y. Shi, and I. Matsuda, Phys. Rev. B **94**, 195134 (2016).
[17] P. Li, Y. Wen, X. He, Q. Zhang, C. Xia, Z.-M. Yu, S. A. Yang, Z. Zhu, H. N. Alshareef, and X.-X. Zhang, Nat. Commun. **8**, 2150 (2017).
[18] M. N. Ali, J. Xiong, S. Flynn, J. Tao, Q. D. Gibson, L. M. Schoop, T. Liang, N. Haldolaarachchige, M. Hirschberger, N. P. Ong, and R. J. Cava, Nature **514**, 205 (2014).

[19] K. G. Rana, F. K. Dejene, N. Kumar, C. R. Rajamathi, K. Sklarek, C. Felser, and S. S. P. Parkin, Nano Lett. **18**, 6591 (2018).
[20] A. Tiwari, F. Chen, S. Zhong, E. Drueke, J. Koo, A. Kaczmarek, C. Xiao, J. Gao, X. Luo, Q. Niu, Y. Sun, B. Yan, L. Zhao, and A. W. Tsen, Nat. Commun. **12**, 2049 (2021).
[21] K. Kang, T. Li, E. Sohn, J. Shan, and K. F. Mak, Nat. Mater. **18**, 324 (2019).
[22] B. E. Brown, Acta Crystallogr. **20**, 268 (1966).
[23] Y. Zhou, X. Chen, N. Li, R. Zhang, X. Wang, C. An, Y. Zhou, X. Pan, F. Song, B. Wang, W. Yang, Z. Yang, and Y. Zhang, AIP Adv. **6**, 075008 (2016).
[24] Y. Tao, J. A. Schneeloch, A. A. Aczel, and D. Louca, Phys. Rev. B **102**, 060103 (2020).
[25] S. Ji, O. Grånäs, and J. Weissenrieder, ACS Nano **15**, 8826 (2021).
[26] T. Fukuda, K. Makino, Y. Saito, P. Fons, A. V. Kolobov, K. Ueno, and M. Hase, Appl. Phys. Lett. **116**, 093103 (2020).
[27] M.-X. Guan, E. Wang, P.-W. You, J.-T. Sun, and S. Meng, Nat. Commun. **12**, 1885 (2021).
[28] K. Nassau, *The Physics and Chemistry of Color*, 2nd ed. (Wiley, New York, 2001).
[29] D. Hirai, T. Yajima, D. Nishio-Hamane, C. Kim, H. Akiyama, M. Kawamura, T. Misawa, N. Abe, T.-h. Arima, and Z. Hiroi, J. Am. Chem. Soc. **139**, 10784 (2017).
[30] Y.-M. Chang, L. Xu, and H. W. K. Tom, Chem. Phys. **251**, 283 (2000).
[31] A. J. Frenzel, C. C. Homes, Q. D. Gibson, Y. M. Shao, K. W. Post, A. Charnukha, R. J. Cava, and D. N. Basov, Phys. Rev. B **95**, 245140 (2017).
[32] S.-i. Kimura, Y. Nakajima, Z. Mita, R. Jha, R. Higashinaka, T. D. Matsuda, and Y. Aoki, Phys. Rev. B **99**, 195203 (2019).
[33] C. C. Homes, M. N. Ali, and R. J. Cava, Phys. Rev. B **92**, 161109 (2015).
[34] A. N. Domozhirova, A. A. Makhnev, E. I. Shreder, S. V. Naumov, A. V. Lukoyanov, V. V. Chistyakov, J. C. A. Huang, A. A. Semiannikova, P. S. Korenistov, and V. V. Marchenkov, J. Phys.: Conf. Ser. **1389**, 012149 (2019).
[35] F. Hou, D. Zhang, P. Sharma, S. Singh, T. Wu, and J. Seidel, ACS Appl. Electron. Mater. **2**, 2196 (2020).
[36] F. Ye, J. Lee, J. Hu, Z. Mao, J. Wei, and P. X.-L. Feng, Small **12**, 5802 (2016).
[37] Q. Song, X. Pan, H. Wang, K. Zhang, Q. Tan, P. Li, Y. Wan, Y. Wang, X. Xu, M. Lin, X. Wan, F. Song, and L. Dai, Sci. Rep. **6**, 29254 (2016).
[38] H. Wang and X. Qian, npj Comput. Mater. **5**, 119 (2019).
[39] Y. R. Shen, *Principles of Nonlinear Optics* (Wiley, New York, 1984).
[40] E. Drueke, J. Yang, and L. Zhao, Phys. Rev. B **104**, 064304 (2021).
[41] Y. Wu, N. H. Jo, M. Ochi, L. Huang, D. Mou, S. L. Bud'ko, P. C. Canfield, N. Trivedi, R. Arita, and A. Kaminski, Phys. Rev. Lett. **115**, 166602 (2015).
[42] B. He, C. Zhang, W. Zhu, Y. Li, S. Liu, X. Zhu, X. Wu, X. Wang, H.-h. Wen, and M. Xiao, Sci. Rep. **6**, 30487 (2016).
[43] H. J. Zeiger, J. Vidal, T. K. Cheng, E. P. Ippen, G. Dresselhaus, and M. S. Dresselhaus, Phys. Rev. B **45**, 768 (1992).
[44] T. E. Stevens, J. Kuhl, and R. Merlin, Phys. Rev. B **65**, 144304 (2002).
[45] D. Soranzio, M. Peressi, R. J. Cava, F. Parmigiani, and F. Cilento, Phys. Rev. Res. **1**, 032033 (2019).
[46] P. Hein, S. Jauernik, H. Erk, L. Yang, Y. Qi, Y. Sun, C. Felser, and M. Bauer, Nat. Commun. **11**, 2613 (2020).
[47] M. Rhodes, G. Steinmeyer, J. Ratner, and R. Trebino, Laser Photonics Rev. **7**, 557 (2013).
[48] A. N. Afanasiev, A. A. Greshnov, and D. Svintsov, Phys. Rev. B **99**, 115202 (2019).
[49] M. S. Foster and I. L. Aleiner, Phys. Rev. B **79**, 085415 (2009).
[50] Y. Qi, M. Guan, D. Zahn, T. Vasileiadis, H. Seiler, Y. W. Windsor, H. Zhao, S. Meng, and R. Ernstorfer, arXiv:2105.14175 (2021).
[51] M. Kim, S. G. Xu, A. I. Berdyugin, A. Principi, S. Slizovskiy, N. Xin, P. Kumaravadivel, W. Kuang, M. Hamer, R. Krishna Kumar, R. V. Gorbachev, K. Watanabe, T. Taniguchi, I. V. Grigorieva, V. I. Fal'ko, M. Polini, and A. K. Geim, Nat. Commun. **11**, 2339 (2020).